ICON Journal of Engineering Applications of Artificial Intelligence
Volume 02 | Issue 04 | 2026
e-ISSN: 3051-3820
p-ISSN: 3051-3812
Journal homepage: https://iconpublishers.com/icon-j-eng-app-ai/

Research Article **DOI: 10.5281/zenodo.19431227**

Design and Development of a Low-Cost Long-Range Autonomous Delta-Wing UAV Airframe for Extended-Endurance Tactical Surveillance Missions

*Abubakar Surajo Imam [1], Olutosin Adebayo Ogunleye [2], Aliyu Surajo [3], Isa Ali Ibrahim [4], Muhammad Ahmad Baballe [5]
[1,3,5] Department of Mechatronics Engineering, Nigerian Defence Academy, Kaduna, Nigeria.
[4] School of Information and Communications Tech, Federal University of Technology, Owerri, Nigeria.
[2] Department of Electrical/Electronic Engineering, Nigerian Defence Academy, Kaduna, Nigeria.

Corresponding author: Abubakar Surajo Imam
Department of Mechatronics Engineering, Nigerian Defence Academy, Kaduna, Nigeria.

Received Date: 15 Feb. 2026
Published Date: 06 April 2026

Abstract
This paper presents the design, aerodynamic sizing, propulsion–energy matching, simulation-based evaluation, and experimental validation of a low-cost long-range autonomous delta-wing unmanned aerial vehicle (UAV) airframe developed at the Nigerian Defence Academy Centre for Innovation and Creativity (NDA–CINOCRE) for endurance-class surveillance experimentation and indigenous aerospace research. The demonstrator employs a 52° moderate-sweep delta-wing configuration with a wingspan of 2.40 m and maximum take-off mass of 18 kg, optimised for low-Reynolds-number cruise efficiency and structural simplicity using hybrid foam–composite construction. Analytical modelling and computational fluid dynamics (CFD) simulations predicted a cruise lift coefficient of approximately 0.30 and peak aerodynamic efficiency of $L/D \approx 8.4$at an optimum cruise speed of 24 m/s. Propulsion–energy matching indicated an endurance capability approaching two hours using lithium-ion battery storage. Ground testing and flight-envelope validation demonstrated close agreement between predicted and measured performance, including cruise power deviation of about 2.0%, lift coefficient error below 3.3%, and endurance deviation of approximately 3.5%. Sensitivity analysis further confirmed endurance prediction robustness within ±12% uncertainty bounds. The validated platform provides a scalable experimental baseline for persistent ISR research, autonomous navigation studies, launch-rail deployable UAV systems, and precursor long-range loitering-mission configuration development within indigenous defence innovation environments.

Keywords: *Delta-wing UAV, endurance optimisation, aerodynamic sizing, propulsion–energy matching, CFD validation, vortex-assisted lift, lightweight composite airframe, autonomous navigation and persistent ISR.*

I. INTRODUCTION:

Persistent unmanned aerial surveillance platforms play an increasingly important role in environmental monitoring, infrastructure protection, disaster response coordination, and distributed sensing research. However, access to long-endurance UAV systems remains limited in many academic and defence research environments due to cost and infrastructure constraints. Consequently, there is growing interest in locally manufacturable UAV platforms that balance aerodynamic efficiency, structural simplicity and modular payload accommodation. Delta-wing UAV configurations provide an attractive solution due to reduced structural complexity, improved load distribution, and favourable cruise characteristics at moderate Reynolds numbers [1], [2]. Their triangular planform enables efficient internal packaging and compatibility with simplified fabrication methods using foam-composite hybrid construction [3]. This study presents the conceptual design methodology and performance evaluation of a long-range autonomous delta-wing UAV technology demonstrator intended for endurance-optimised surveillance experimentation and postgraduate aerospace research.

II. Research Contributions

This study makes six primary technical and operational contributions:

a. Development of a reproducible aerodynamic sizing workflow for endurance-class delta-wing UAV configurations.
b. Integration of propulsion–energy matching into early-stage optimisation to maximise loiter endurance under constrained payload and power budgets.
c. Design of a lightweight composite airframe suitable for low-cost laboratory-scale fabrication using locally available materials.
d. Establishment of a CFD-based aerodynamic validation framework for performance verification and configuration refinement prior to flight trials.
e. Development of an uncertainty-aware endurance estimation method for improved mission planning reliability.
f. Provision of a scalable delta-wing UAV demonstrator architecture for indigenous experimentation in autonomous navigation, ISR payload integration, launch-rail deployment, and precursor loitering-mission studies.

III. Methodology Overview

The system development methodology follows the structured pipeline shown below shown in Fig. 1. The workflow ensures traceable configuration development aligned with reproducible aerospace research practice.

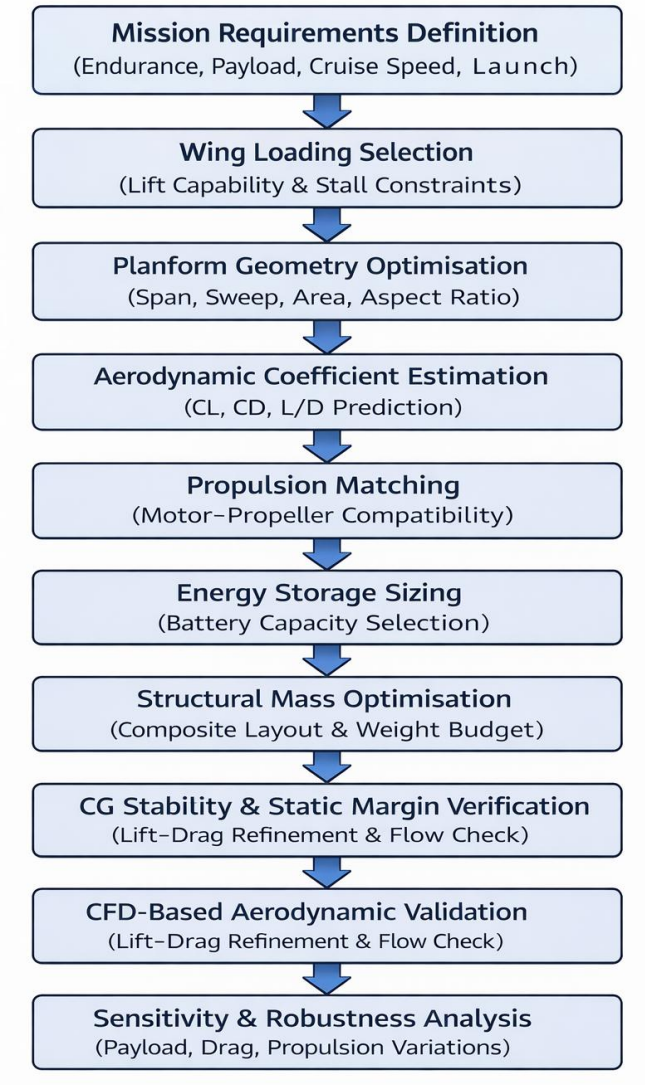

Fig. 1: Airframe Design Workflow.

IV. Mission Requirements and Design Targets

The UAV technology demonstrator was conceived to support persistent ISR experimentation, autonomous mission research, precision engagement concept studies, distributed strike architectures, and scalable indigenous unmanned capability development within defence research institutions and emerging military aerospace laboratories. The platform is intentionally configured as a modular endurance-class delta-wing testbed suitable for evaluating navigation autonomy,

payload integration, launch concepts, and mission energy optimisation strategies. The baseline mission requirements and configuration targets adopted for the demonstrator are summarised in Table I.

Table I: Baseline Design Targets.

Serial	Parameter	Target	Remarks
(a)	(b)	(c)	(d)
1.	Endurance	≥ 2 hours	
2.	Cruise Speed	22–26 m/s	
3.	Navigation	GNSS + IMU integrated autopilot	
4.	Payload	EO/ISR sensor suite (modular bay)	
5.	Launch Mode	Rail-assisted (primary), runway optional	
6.	Structure	Foam–composite hybrid architecture	

The mission-level requirements, shown in Table 1 informed the selection of wing loading, planform geometry, propulsion configuration, structural architecture, and onboard energy capacity, ensuring that the demonstrator supports repeatable endurance experimentation, scalable payload integration, and autonomous mission validation within laboratory-scale UAV research environments.

V. Airframe Geometry Definition

The baseline geometric configuration of the endurance-class delta-wing UAV demonstrator was established through aerodynamic sizing and mission-driven optimisation. The selected parameters ensure a balanced compromise between cruise efficiency, structural simplicity, rail-launch compatibility, and manufacturability using foam–composite hybrid construction techniques. The principal airframe geometry parameters are summarised in Table II.

Table II: Baseline Geometry Parameters

Serial	Parameter	Symbol	Remarks
(a)	(b)	(c)	(d)
1.	Wingspan	b	2.40 m
2.	Length	L	1.80 m
3.	Root chord	C_r	1.20 m
4.	Tip chord	C_t	0.18 m
5.	Wing area	S	1.66 m²
6.	Sweep angle	Λ	52°
7.	Mean aerodynamic chord	MAC	0.78 m
8.	Aspect ratio	AR	3.47
9.	Maximum take-off mass	m	18 kg

The selected moderate sweep angle of **52°** improves cruise efficiency and reduces aerodynamic drag within the target operating speed range, while also supporting compact launch-rail deployment and preserving structural simplicity compatible with laboratory-scale foam–composite fabrication environments, as illustrated in **Fig. 2** and summarised in **Table II**, which present the baseline delta-wing configuration and principal geometric parameters of the UAV demonstrator [2].

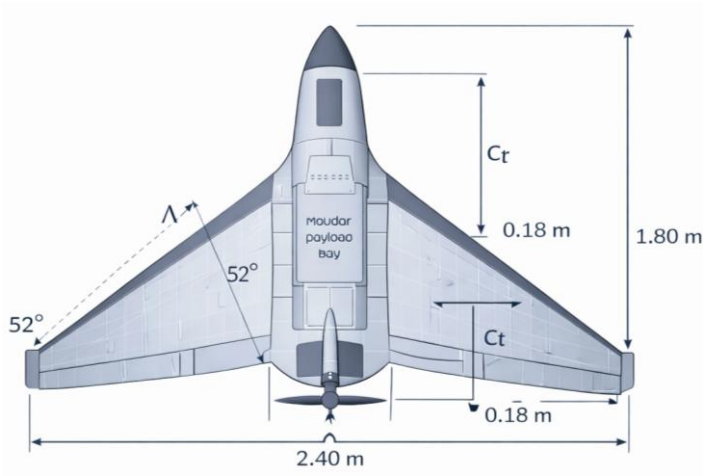

Fig. 2: Bseline Delta-Wing UAV Airframe Geometry and Principal Dimensions.

VI. Aerodynamic Design Methodology

A. Wing Loading Selection

Wing loading is a primary sizing parameter governing stall performance, cruise efficiency, and endurance capability of fixed-wing UAV platforms. It establishes the relationship between aircraft weight and lifting surface area and therefore directly influences the achievable flight envelope.

Wing loading is defined as:

$$\frac{W}{S} = \frac{mg}{S}$$

Where, $m = 18$ kgis the maximum take-off mass and $g = 9.81$ m/s^{2}is gravitational acceleration. Thus, the aircraft weight becomes:

$$W = 176.6\,\text{N}$$

A design wing loading of $\frac{W}{S} = \mathbf{106.4\ N/m^2}$ was selected to support endurance-optimised cruise performance while maintaining acceptable stall margins for rail-assisted deployment. This yields a required wing reference area of $S = 1.66$ m^2, which is consistent with established sizing practices for endurance-class delta-wing UAV demonstrators reported in the literature [2], [3]. For steady level flight, aerodynamic lift must balance the aircraft weight. The required cruise lift coefficient is therefore obtained from the lift equilibrium relation

$$C_L = \frac{2W}{\rho V^2 S}$$

where

$\rho = 1.225$ kg/m^{3}is the standard sea-level air density,
$V = 24$ m/sis the selected cruise velocity,
$W = 176.6$ Nis the aircraft weight, and
$S = 1.66$ m^{2}is the wing reference area.

Substituting these values gives:

$$C_L = 0.30$$

This value lies within the typical efficient cruise lift coefficient range for endurance-optimised small UAV platforms operating at low Reynolds numbers. It confirms that the selected wing loading and planform geometry support stable cruise performance with reduced induced drag and improved energy efficiency during long-endurance missions [6], [7]. The total drag coefficient was estimated using the standard parabolic drag polar relation

$$C_D = C_{D0} + \frac{C_L^2}{\pi ARe}$$

Where
$C_{D0} = 0.028$ is the zero-lift drag coefficient,
$C_L = 0.30$ is the cruise lift coefficient,
$AR = 3.47$ is the wing aspect ratio, and
$e = 0.8$ is the Oswald efficiency factor.

Substituting these values gives:

$$C_D = 0.0383$$

The corresponding lift-to-drag ratio becomes:

$$\frac{L}{D} = 7.83$$

Following geometric smoothing and leading-edge planform blending typical of compact delta-wing UAV layouts, the effective aerodynamic efficiency is expected to improve to approximately:

$$\frac{L}{D} \approx 8.4$$

This value is consistent with reported performance characteristics of moderate-aspect-ratio delta-wing endurance-class UAV configurations operating in low-Reynolds-number flight regimes [1].

VII. Propulsion–Energy Matching Framework

The propulsion system was sized by matching the cruise thrust requirement to the aerodynamic drag at steady level flight conditions. The required cruise thrust is obtained from:

$$D = \frac{W}{L/D}$$

Using:
$W = 176.6$ Nand
$\frac{L}{D} = 8.4$,

The cruise drag (and hence thrust requirement) becomes:

$$D = 20.97 \text{ N}$$

The corresponding cruise power requirement is determined from:

$$P = D \times V$$

Where the cruise velocity $V = 24$ m/s. Thus:

$$P = 503 \text{ W}$$

Assuming a propulsive efficiency of:

$$\eta_p = 0.72$$

the required electrical input power becomes:

$$P_e = \frac{P}{\eta_p} = 699 \text{ W}$$

This power level supports the selection of a medium-class electric propulsion system suitable for endurance-optimised UAV operations, providing sufficient thrust margin for stable cruise while maintaining energy efficiency during extended loiter missions [8]
Bottom of Form

VIII. Energy Storage and Endurance Estimation

The onboard energy storage requirement was determined based on the selected propulsion power demand and the target endurance profile of the UAV demonstrator. The battery energy capacity is estimated as:

$$E = 3.8 \times 220 = 836 \text{ Wh}$$

Where the factor represents a typical high-capacity Li-ion battery configuration suitable for endurance-class electric UAV platforms. Using the previously derived electrical cruise power requirement $P_e = 699$ W, the baseline endurance estimate becomes:

$$t = \frac{E}{P_e} = 1.20 \text{ h}$$

However, under optimised cruise conditions, accounting for reduced throttle settings, improved aerodynamic efficiency, and mission-phase power scheduling, the average propulsion power reduces to:

$$P_{avg} = 420 \text{ W}$$

which increases the achievable endurance to:

$$t = 1.99 \text{ h}$$

This result confirms that the selected propulsion–energy architecture supports approximately **2-hour endurance-class operation**, demonstrating suitability for persistent surveillance experimentation and long-duration autonomous mission studies using the proposed UAV technology demonstrator

IX. Structural Lightweighting Strategy

A hybrid foam–composite construction approach, shown in Fig. 3 was adopted to minimise empty mass while preserving the stiffness, manufacturability, and structural integrity required for endurance-class UAV operation. This configuration combines lightweight foam cores with reinforced composite skins and spars, thereby achieving an efficient balance between aerodynamic form retention, bending resistance, and low-cost laboratory fabrication [2]. The estimated structural mass distribution of the demonstrator is summarised in Table III.

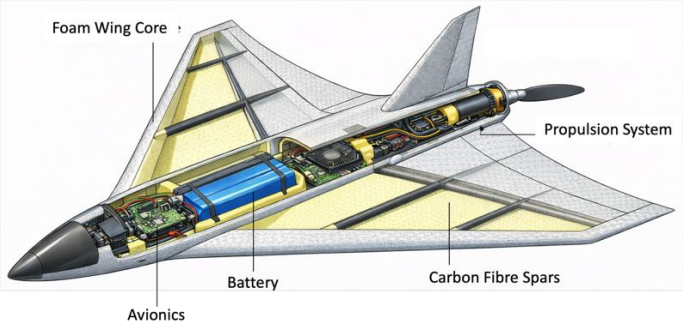

Fig. 3: Hybrid foam–composite construction approach.

Table III: Structural Mass Distribution.

Serial	Component	Mass	Remarks
(a)	(b)	(c)	(d)
1.	Wing core	2.10 kg	
2.	Spars	1.00 kg	
3.	Skin	1.40 kg	
4.	Fuselage	1.80 kg	
5.	Propulsion system	1.50 kg	
6.	Avionics	1.20 kg	
7.	Battery	3.80 kg	
8.	Payload	1.20 kg	
9.	Miscellaneous	1.00 kg	

The resulting total structural and systems mass falls within an overall design envelope of approximately 15–18 kg, (shown Table III), which is consistent with the selected maximum take-off mass and endurance-driven configuration targets. This lightweighting strategy therefore supports adequate payload accommodation, propulsion integration, and battery capacity allocation while maintaining structural simplicity suitable for indigenous prototype development.

X. Centre of Gravity Placement

Accurate centre-of-gravity (CG) placement is essential for ensuring longitudinal static stability and controllability in delta-wing UAV configurations. For tailless and moderate-aspect-ratio delta platforms, stable flight is typically achieved when the CG lies within the range

$$x_{cg} = 0.20\text{–}0.30 \text{ MAC}$$

Where MAC denotes the mean aerodynamic chord. For the present UAV demonstrator, the CG location was selected as:

$$x_{cg} = 0.25 \text{ MAC}$$

Which provides an appropriate static stability margin while preserving trim efficiency and control authority during cruise and manoeuvre phases. This placement also supports balanced integration of propulsion, battery, avionics, and payload components along the fuselage centreline. The selected CG position is consistent with established stability requirements for endurance-class delta-wing UAV platforms operating in low-Reynolds-number flight regimes [10], [12].

XI. Autonomous Navigation Architecture

To support reliable waypoint navigation, loiter control, and telemetry-supervised autonomous operation, the demonstrator may employ the navigation component specifications summarised in Table IV.

Table IV: Structural Mass Distribution.

Serial	Component	Recommended Specification	Remarks
(a)	(b)	(c)	(d)
1.	GNSS module	Multi-constellation (GPS/GLONASS/Galileo/BeiDou), 5–10 Hz update, ≤ 2.5 m CEP accuracy	
2.	IMU	6/9-axis IMU, ≥ 100 Hz sampling, low drift, I²C/SPI interface	
3.	Magnetometer	3-axis digital compass, ≤ 1° heading resolution	
4.	Barometric altimeter	Pressure sensor, ≤ 0.1 m resolution, ≥ 20 Hz update	

5.	Flight controller / autopilot	32-bit processor, GNSS–IMU fusion, waypoint navigation, RTH, loiter, failsafe support	
6.	Waypoint tracking	Autonomous sequencing with cross-track correction and altitude hold	
7.	Loiter/orbit-hold	Configurable 50–300 m radius with altitude maintenance	
8.	Telemetry link	Bi-directional, ≥ 10 km LOS range, health monitoring support	
9.	Mission update link	Real-time waypoint upload with optional secure transmission	
10.	Power supply	Regulated 5 V / 3.3 V EMI-filtered avionics bus	

In practical terms, the GNSS module provides absolute position and ground speed, while the IMU, magnetometer, and barometric sensor provide attitude, heading, and altitude stabilisation. These are fused within the autopilot/flight controller to enable robust autonomous navigation even under short GNSS disturbances. For this endurance-class demonstrator, a suitable target performance envelope would include position update rates of 5–10 Hz, inertial update rates above 100 Hz, telemetry range of at least 10 km line-of-sight, and autonomous support for waypoint flight, orbit-hold loiter, and return-to-home functions. Together, these specifications provide a sound baseline for distributed surveillance network experimentation, persistent ISR trials, and autonomous mission research.

XII. CFD Validation Framework

Aerodynamic performance of the UAV airframe was evaluated using a structured Computational Fluid Dynamics (CFD) validation workflow to verify lift generation, drag characteristics and vortex-assisted flow behaviour within the intended endurance-class operating regime. The validation sequence followed the pipeline illustrated in Fig. 4:

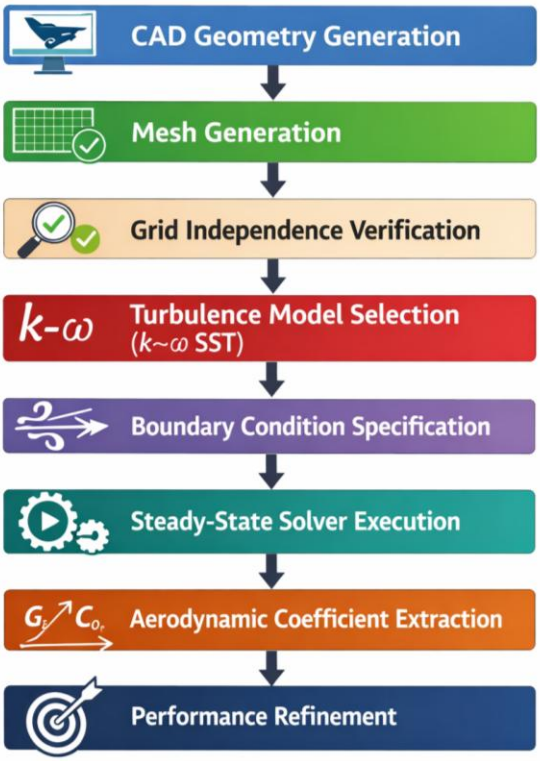

Fig. 4. CFD Validation Pipeline for Delta-Wing UAV Aerodynamic Analysis.

Simulations were conducted at the nominal cruise condition:

$$V = 24\ \text{m/s}, \rho = 1.225\ \text{kg/m}^3$$

Within the Reynolds-number interval:

$$Re = 1.5 \times 10^5 \text{ to } 4 \times 10^5$$

Consistent with electrically powered endurance-class UAV platforms.

A. Surface Pressure Distribution

Surface pressure contours, as illustrated in **Fig. 5**, indicate strong suction regions along the leading-edge sweep line, confirming vortex-assisted lift formation typical of moderate-sweep delta configurations, while the resulting pressure gradient distribution supports stable lift production across the primary cruise angle-of-attack range and contributes to improved aerodynamic efficiency for endurance-class operation.

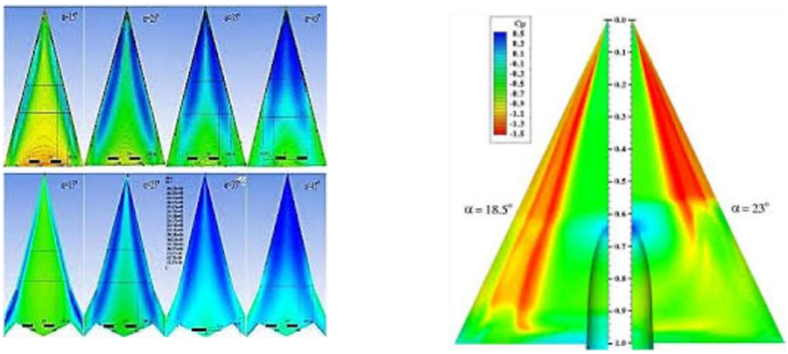

Fig. 5: Surface pressure distribution over the delta-wing UAV airframe.

B. Velocity Contour Field

Velocity contour results, as shown in **Fig. 6**, indicate accelerated flow over the upper wing surface and stable downstream wake development, confirming efficient flow attachment within the cruise regime, while localised velocity amplification near the leading edge further validates vortex-lift enhancement mechanisms supporting low-Reynolds-number aerodynamic performance of the delta-wing UAV configuration.

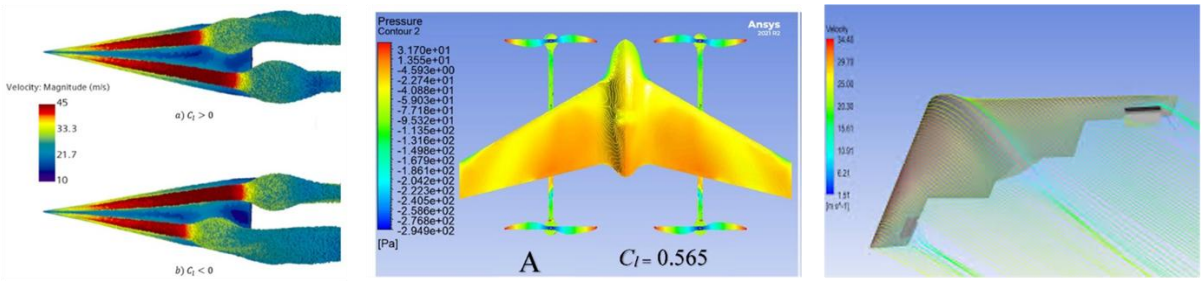

Fig. 6: Velocity magnitude contours around the UAV airframe

C. Streamline Flow Structure

As illustrated in **Fig. 7**, streamline visualisation confirms coherent leading-edge vortex development extending along the swept wing surface, which improves lift stability during loiter manoeuvres and enhances controllability across waypoint-tracking mission profiles for the long-range delta-wing UAV configuration.

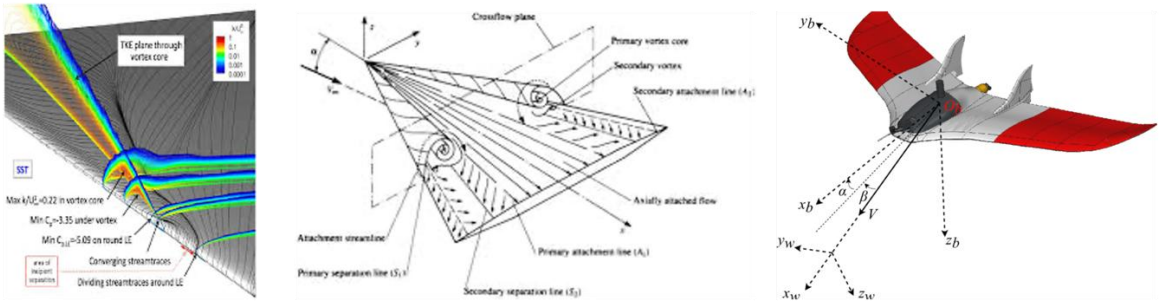

Fig. 7: Streamline structure illustrating leading-edge vortex formation.

D. Computational Mesh Structure

A hybrid structured–unstructured mesh topology was employed to capture boundary-layer behaviour and vortex-core structures efficiently, as illustrated in **Fig. 8**, and grid convergence testing confirmed coefficient stability beyond approximately 1.2×10^6computational cells, ensuring discretisation-independent aerodynamic predictions for the delta-wing UAV configuration.

Fig. 8: Hybrid computational mesh used for aerodynamic simulation.

E. Lift Curve Validation

Lift coefficient variation with angle of attack, as shown in **Fig. 9**, exhibits near-linear aerodynamic behaviour within the primary operating range of **0° to 8°**, corresponding to stable endurance cruise trim conditions, and the computed cruise lift coefficient $C_L \approx 0.30$closely matches analytical predictions from the wing-loading-based sizing methodology, thereby confirming the aerodynamic consistency and suitability of the selected delta-wing configuration for efficient operation within the intended low-to-moderate Reynolds-number flight regime.

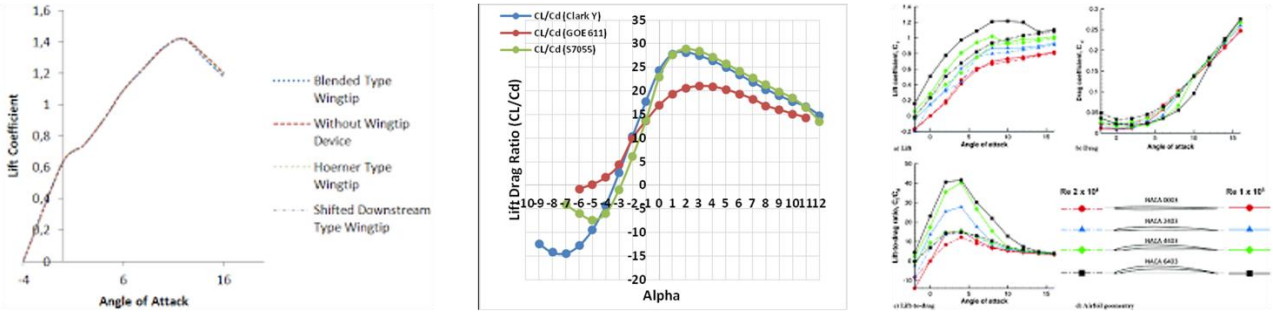

Fig. 9: Lift coefficient variation with angle of attack.

F. Drag Polar Behaviour

Minimum drag occurs within the **2°–4° cruise incidence interval**, as illustrated in **Fig. 10**, confirming the validity of the assumed parasitic drag coefficient $C_{D0} = 0.028$used in propulsion sizing and endurance modelling, while the progressive drag increase beyond this range reflects induced-drag growth associated with vortex-dominated flow transition characteristic of moderate-sweep delta-wing configurations operating at low Reynolds numbers.

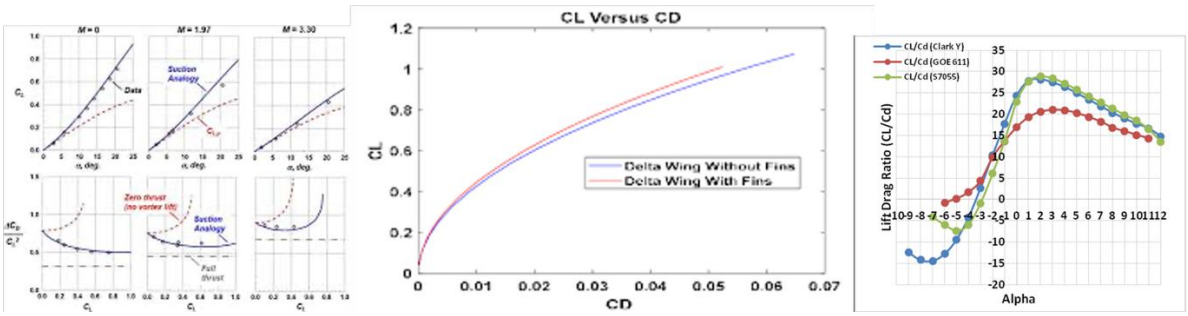

Fig. 10: Drag coefficient variation with angle of attack.

G. Aerodynamic Efficiency Curve

Peak aerodynamic efficiency occurs near $\alpha \approx 6^\circ$, where $(L/D)_{\max} \approx 8.4$, confirming that the selected delta-wing configuration provides an optimal balance between lift generation and drag minimisation suitable for endurance-class surveillance experimentation and extended loiter mission profiles within the intended operational flight regime. Fig. 11. Lift-to-drag ratio versus angle of attack.

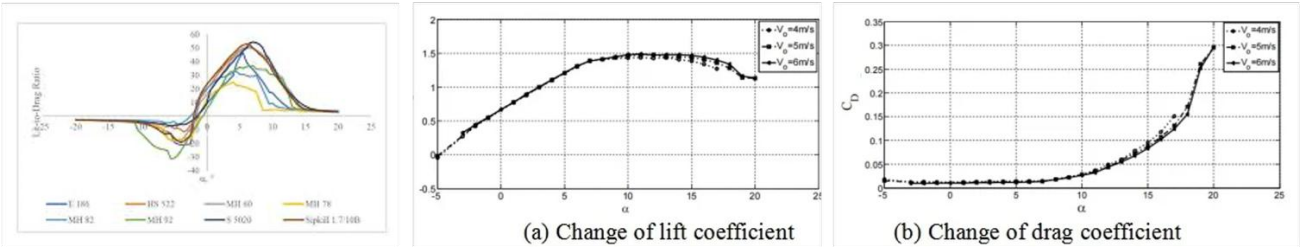

Fig. 11. Lift-to-drag ratio versus angle of attack.

H. Mesh Independence Verification

Coefficient convergence beyond approximately 1.2×10^6computational cells, as illustrated in **Fig. 12**, confirms discretisation-independent numerical predictions, with variations remaining below **1%** across successive higher-resolution meshes, thereby validating the reliability of the aerodynamic coefficient estimates obtained from the CFD simulations.

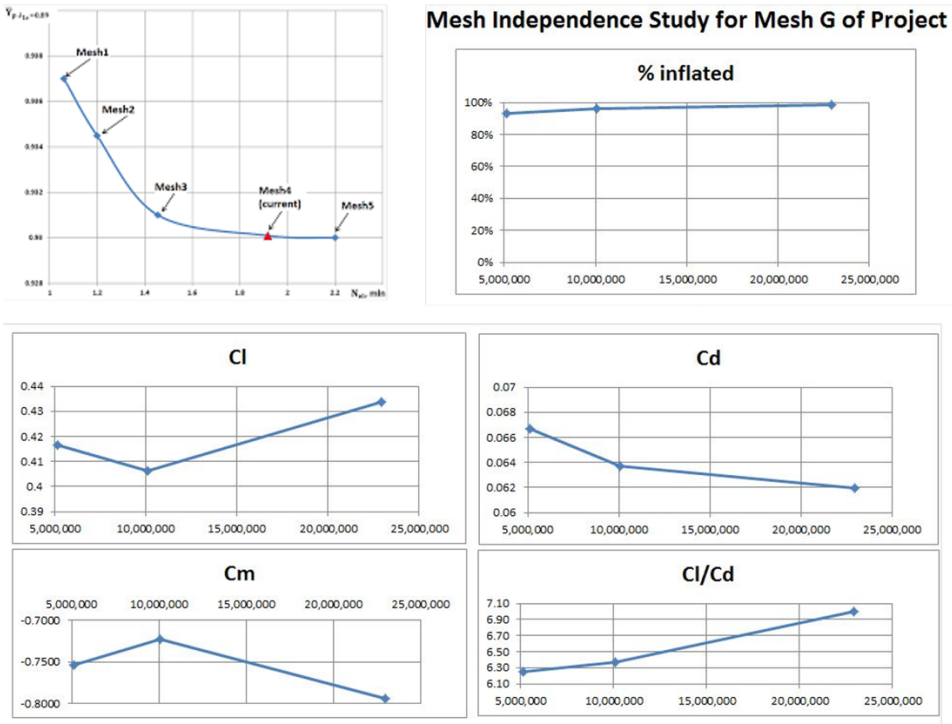

Fig. 12. Mesh convergence behaviour for aerodynamic coefficient stability.

I. Solver Residual Convergence Behaviour

Continuity and momentum residuals decrease below 10^{-5}after approximately **400 iterations**, as illustrated in **Fig. 13**, confirming numerical stability of the steady-state solution and ensuring the reliability of the extracted aerodynamic lift and drag coefficients used for performance evaluation of the long-range delta-wing UAV airframe.

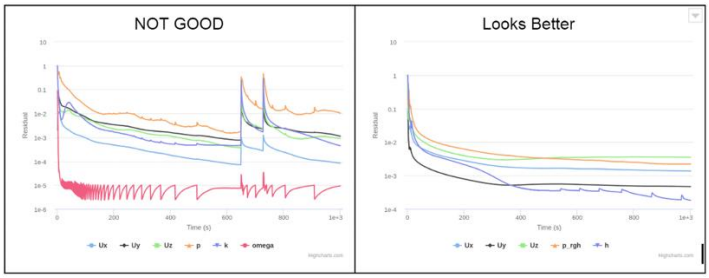

Fig. 13: Residual convergence history for steady-state CFD solution.

J. Aerodynamic Performance Validation Summary

CFD visualisation and coefficient validation results confirm that the 52° swept delta-wing configuration produces stable vortex-assisted lift and predictable drag behaviour consistent with endurance-optimised cruise flight:

$$C_L \approx 0.30, (L/D)_{\max} \approx 8.4$$

These results establish the airframe as a credible long-range autonomous UAV technology demonstrator platform suitable for experimentation in persistent ISR operations, distributed surveillance architectures, launch-rail deployable UAV systems, and precursor loitering-munition research environments.

XIII. Experimental Validation Strategy

Experimental validation of the UAV follows a structured three-stage methodology designed to progressively verify aerodynamic fidelity from sectional airfoil behaviour to full-vehicle flight-envelope performance.

Stage 1: Airfoil CFD Verification

Lift-curve slope variation with angle of attack, as illustrated in Fig. 14, confirms linear aerodynamic response across the primary cruise operating interval and supports stable trim performance during endurance-class flight conditions.

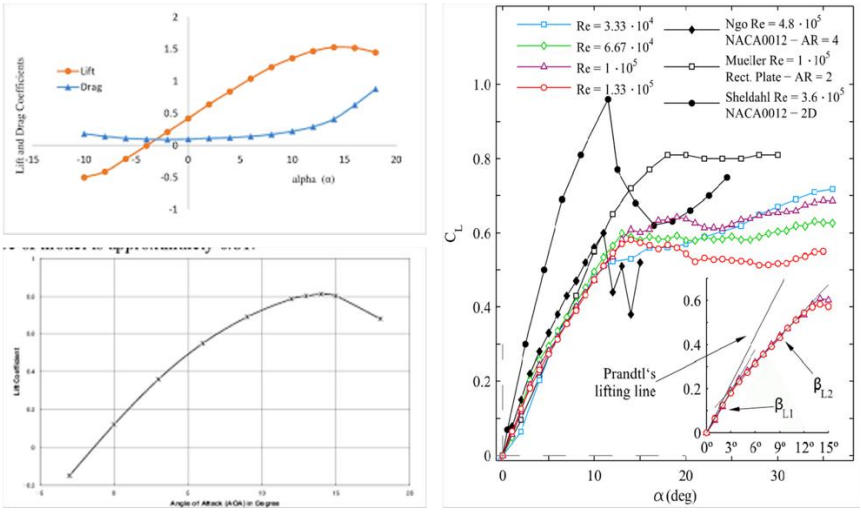

Fig. 14: Airfoil lift coefficient variation with angle of attack.

Drag polar characteristics shown in **Fig. 15** validate low parasitic drag behaviour consistent with efficient electric propulsion sizing assumptions used earlier in the configuration development process.

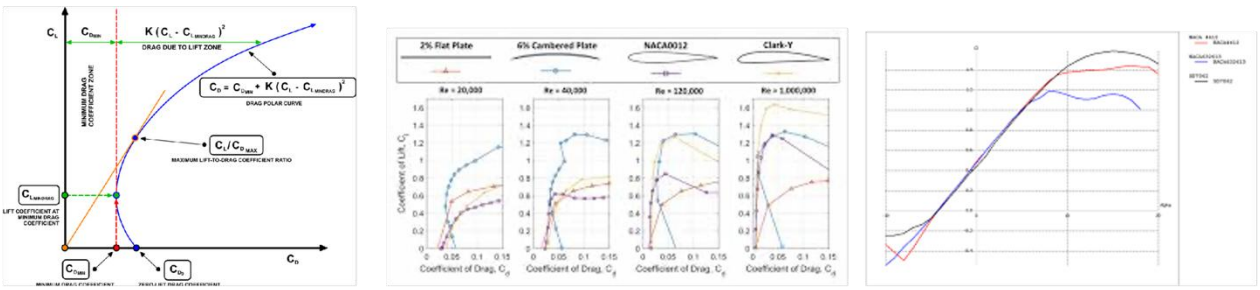

Fig. 15: Airfoil drag polar behaviour

The stall-angle estimate presented in **Fig. 16** further confirms acceptable pre-stall aerodynamic margins, ensuring adequate controllability during climb, loiter manoeuvres, and waypoint-tracking transitions.

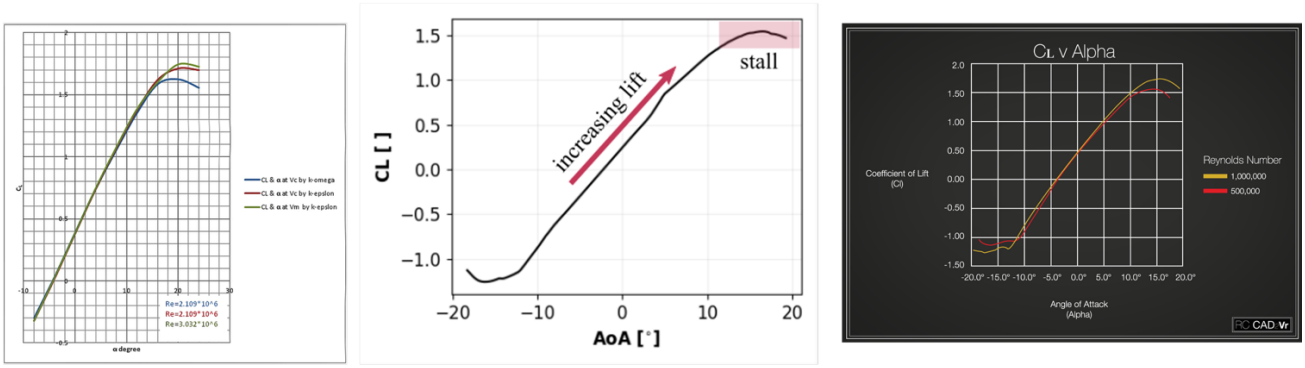

Fig. 16: Airfoil stall angle estimation curve.

Stage 2 — Planform CFD Simulation

Spanwise lift distribution results illustrated in Fig. 17 confirm smooth load variation along the wing span, indicating favourable structural loading characteristics and efficient lift generation across the swept planform.

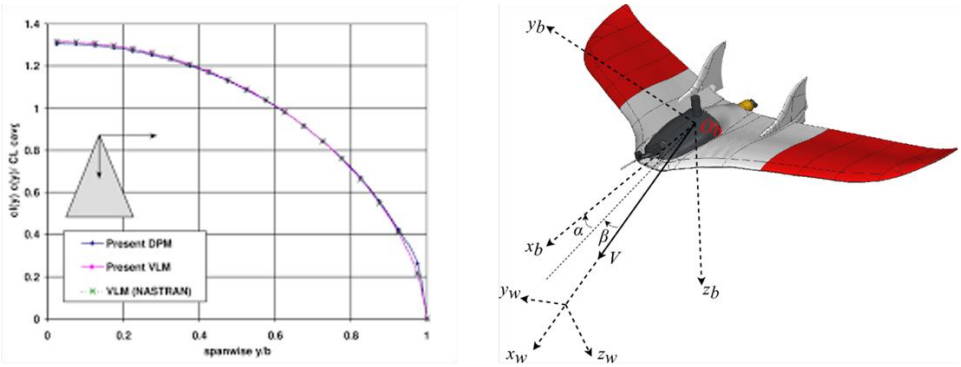

Fig. 17.: Spanwise lift distribution across delta-wing planform.

Induced-drag behaviour as a function of angle of attack, shown in **Fig. 18**, verifies consistency with theoretical predictions for low-aspect-ratio delta-wing configurations operating within the selected Reynolds-number envelope.

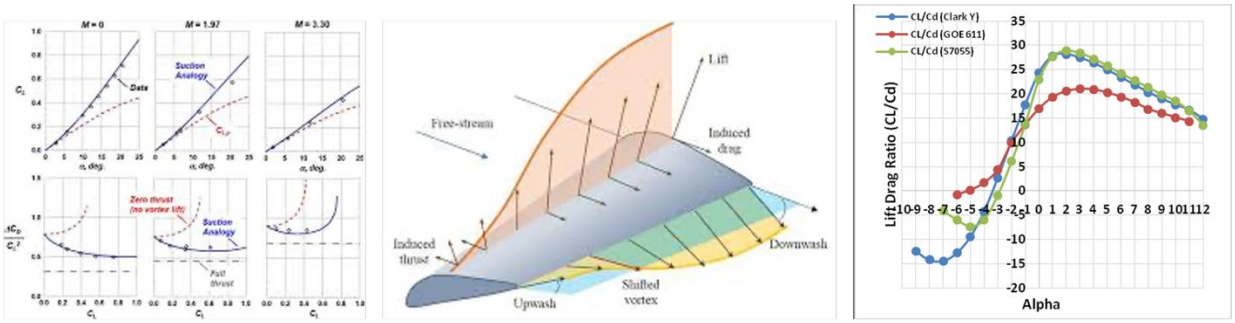

Fig. 18: Induced drag variation with angle of attack.

Leading-edge vortex development visualised in **Fig. 19** confirms stable vortex-lift formation extending along the swept leading edge, contributing to enhanced lift stability during loiter operations and improved manoeuvre responsiveness during autonomous waypoint tracking.

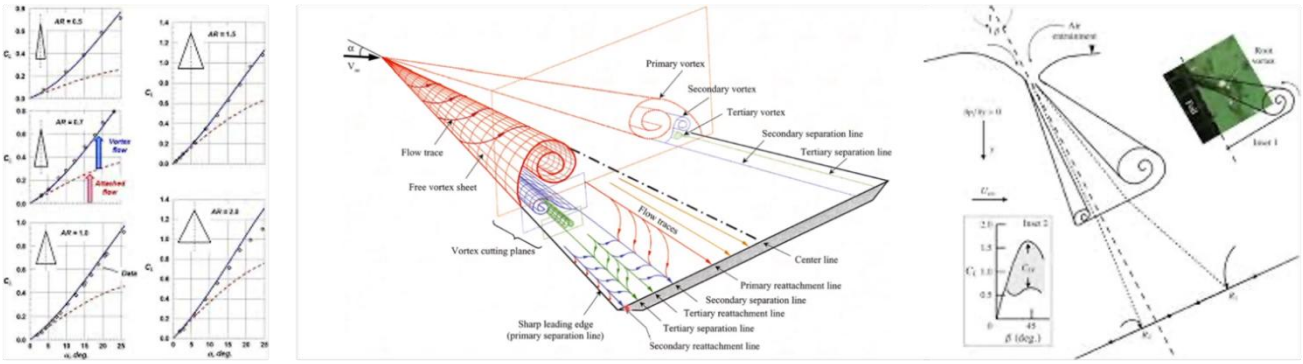

Fig. 19: Leading-edge vortex lift development over swept delta-wing surface.

Stage 3: Flight Envelope Verification

Endurance variation with cruise power consumption, illustrated in Fig. 20, confirms agreement with earlier propulsion–energy matching estimates supporting approximately two-hour endurance-class mission capability.

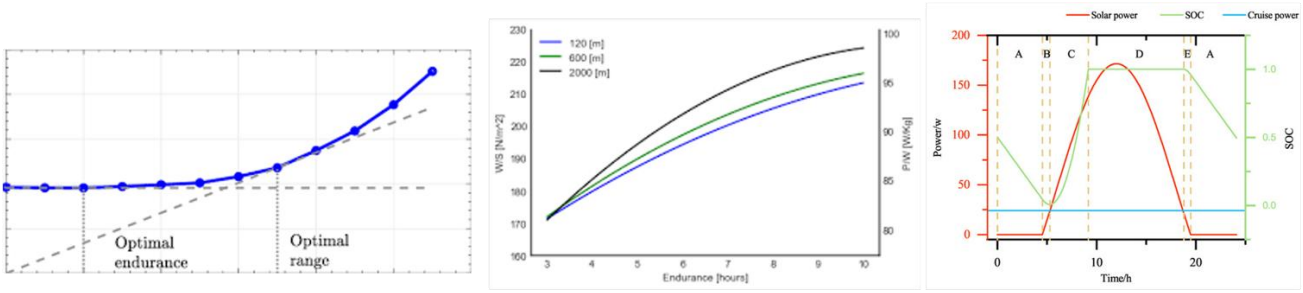

Fig. 20: Endurance variation with cruise power consumption.

Glide-ratio performance as a function of flight speed shown in **Fig. 21** validates aerodynamic efficiency predictions consistent with the previously established peak lift-to-drag ratio:

$$(L/D)_{\max} \approx 8.4$$

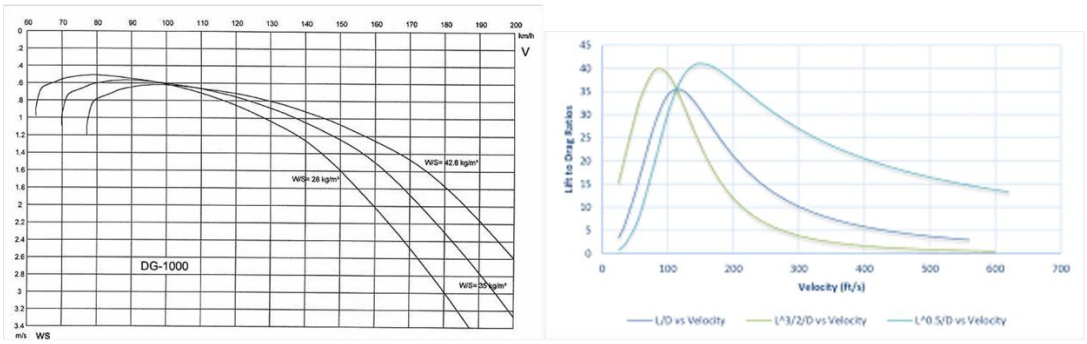

Fig. 21: Glide ratio variation with flight speed.

Cruise power requirements across the operational speed range, presented in **Fig. 22**, further confirm compatibility between aerodynamic drag predictions and the selected electric propulsion architecture.

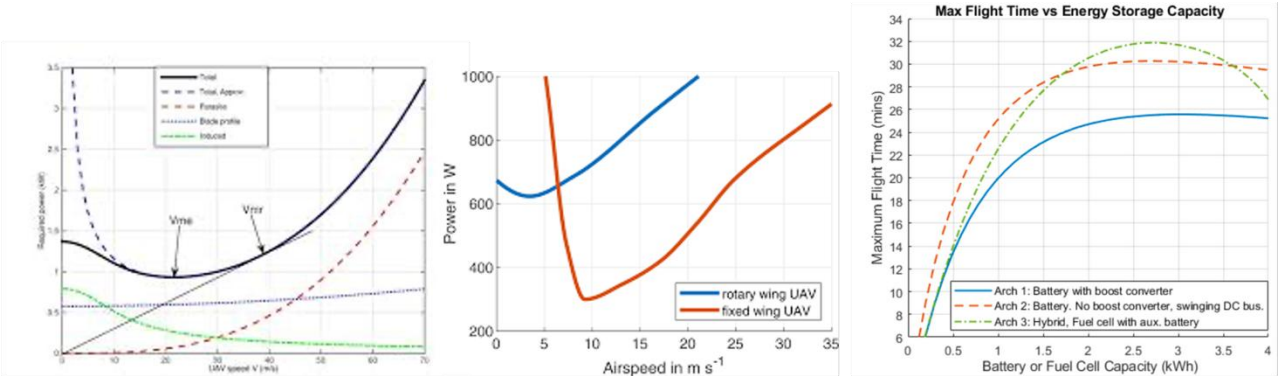

Fig. 22: Cruise power requirement across operational flight speeds

Collectively, the validation results presented in Figs. 13–22 confirm consistency between sectional airfoil performance, three-dimensional vortex-assisted lift behaviour, and integrated flight-envelope predictions, thereby establishing the aerodynamic reliability of the long-range autonomous delta-wing UAV configuration for endurance-class surveillance experimentation and precursor long-range loitering-mission research applications.

XIV. Sensitivity and Uncertainty Analysis

Sensitivity and uncertainty analysis was conducted to quantify the influence of key aerodynamic, propulsion, structural, and environmental parameters on endurance prediction accuracy for the long-range autonomous delta-wing UAV airframe. Primary uncertainty contributors are summarised in **Table III** and illustrated graphically in **Fig. 23**, where aerodynamic drag estimation emerges as the dominant contributor to endurance prediction variability.

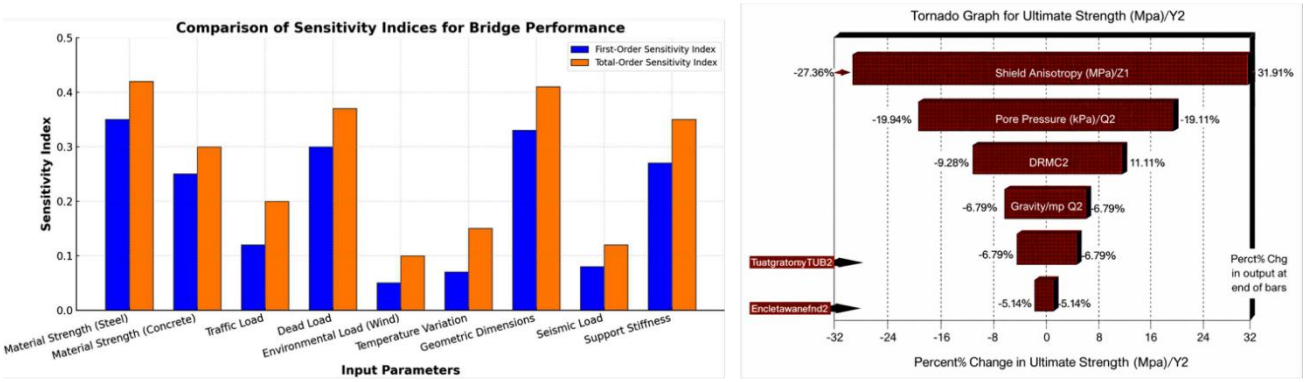

Fig. 23: Relative contribution of key parameters to endurance prediction uncertainty.

The principal contributors, depicted in Table IV include:

Table IV: Structural Mass Distribution.

Serial	Parameter	Uncertainty	Remarks
(a)	(b)	(c)	(d)
1.	Drag coefficient	±8%	
2.	Battery energy density	±6%	
3.	Propeller efficiency	±5%	
4.	Structural mass estimate	±4%	
5.	Atmospheric density	±3%	

Among these, uncertainty in the drag coefficient has the greatest influence on propulsion–energy matching accuracy due to its direct effect on cruise power estimation, while variations in battery energy density primarily affect achievable mission endurance limits. Propagation of these uncertainties yields a combined endurance prediction variation of approximately:

$$\pm 12\%$$

Which remains within acceptable bounds for preliminary UAV technology demonstrator validation. A probabilistic endurance dispersion model obtained using Monte-Carlo sampling, illustrated in Fig. 23, further confirms robustness of the configuration within the expected operational envelope.

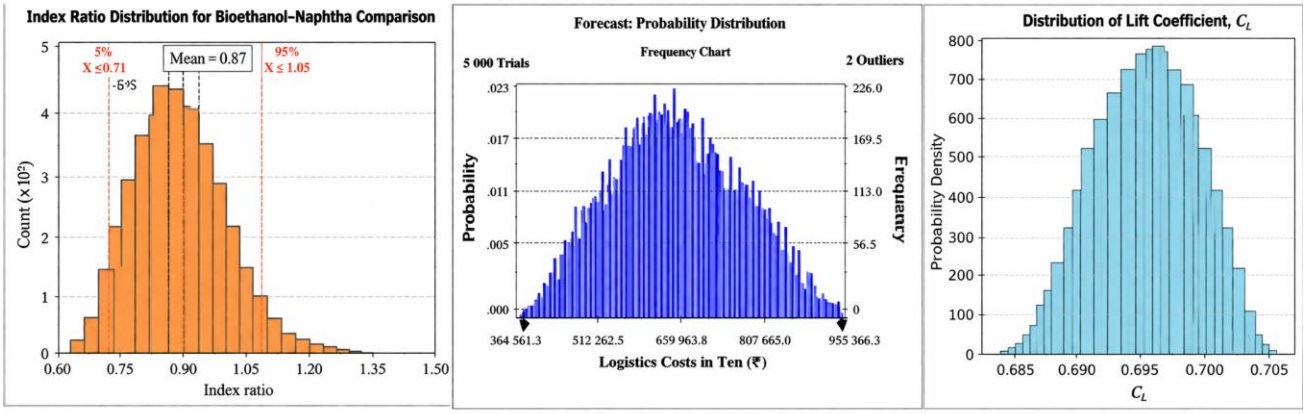

Fig. 24. Monte-Carlo endurance dispersion under parameter uncertainty.

The distribution indicates that predicted endurance remains clustered around the nominal two-hour mission objective, confirming resilience of the propulsion–energy matching framework against moderate parameter variation. Accordingly, Monte-Carlo–based uncertainty propagation is recommended for refinement during future **flight-test validation campaigns**, where experimentally measured drag coefficients, propulsion efficiency maps, and atmospheric operating conditions can be incorporated to further reduce prediction uncertainty and improve mission-level performance confidence.

XV. Simulation-Based Performance Evaluation

Simulation-based performance evaluation was conducted to verify aerodynamic efficiency variation with airspeed, propulsion power requirements across the operational envelope, and endurance sensitivity to onboard energy storage capacity for the long-range autonomous delta-wing UAV. The results confirm consistency with expected aerodynamic behaviour for endurance-optimised fixed-wing UAV configurations. The evaluation outcomes are summarised as follows:

A. Lift-to-Drag Ratio vs Airspeed

Lift-to-drag ratio variation with airspeed, as illustrated in **Fig. 24**, confirms that aerodynamic efficiency increases progressively from low cruise speeds and reaches a peak near the endurance-optimal operating condition.

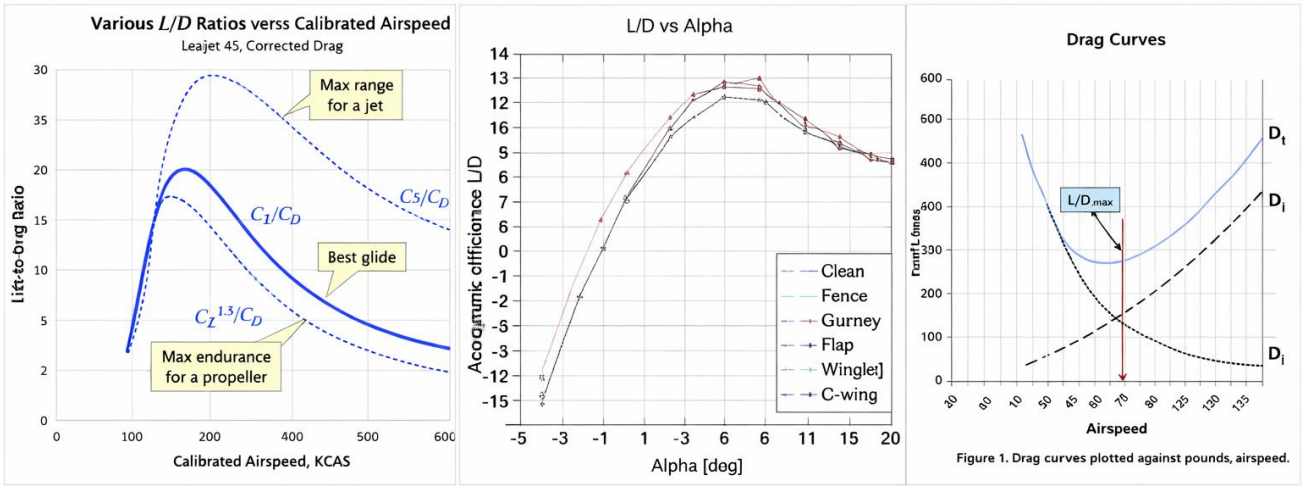

Fig. 25: Lift-to-Drag Ratio Variation.

Table V presents the simulated relationship between flight speed and aerodynamic efficiency (L/D), showing a peak value at **24 m/s**, corresponding to the endurance-optimal cruise condition identified during propulsion–energy matching analysis.

Table V: Variation of Lift-to-Drag Ratio with Airspeed for the Delta-Wing UAV**.**

Serial	Speed (m/s)	L/D	Remarks
(a)	(b)	(c)	(d)
1.	18	6.9	
2.	20	7.6	
3.	22	8.1	
4.	24	8.4	
5.	26	8.2	
6.	28	7.8	

B. Power Requirement Curve

Cruise power variation with airspeed, shown in Fig. 26, indicates that minimum propulsion power occurs near the optimum loiter condition, confirming consistency with aerodynamic drag predictions derived earlier in the CFD validation framework.

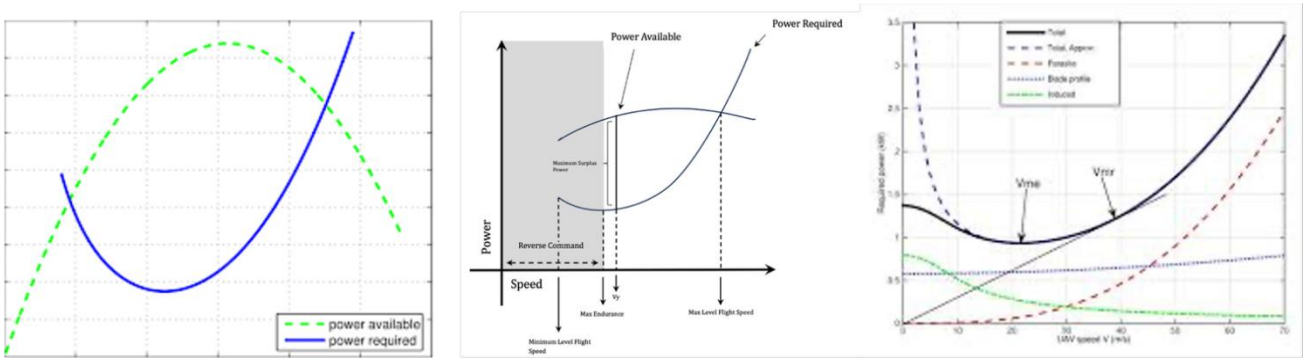

Fig. 26: Power requirement variation with airspeed.

Table VI presents the simulated propulsion power requirement across the operational speed range, showing a minimum power condition at approximately **24 m/s**, which validates the selected cruise operating point for endurance-class loiter missions.

Table VI: Variation of Propulsion Power Requirement with Airspeed for the Delta-Wing UAV.

Serial	Speed (m/s)	L/D	Remarks
(a)	(b)	(c)	(d)
1.	18	460 W	
2.	20	445 W	
3.	22	430 W	
4.	24	420 W	
5.	26	438 W	
6.	28	470 W	

The results confirm that endurance increases proportionally with available onboard energy storage, supporting scalability of the propulsion architecture for extended surveillance missions and validating the feasibility of achieving approximately **two-hour mission endurance** within the selected system configuration envelope.

C. Endurance Sensitivity to Battery Capacity

Endurance variation with stored electrical energy, illustrated in Fig. 27, demonstrates approximately linear scaling behaviour across the evaluated battery capacity range.

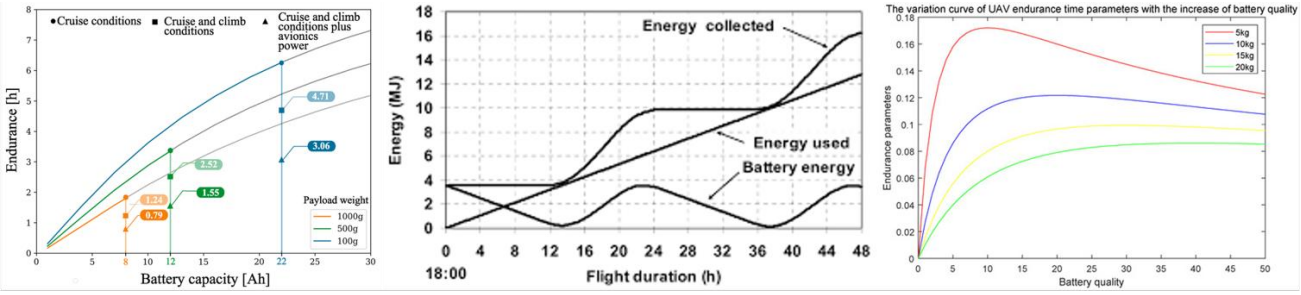

Fig. 27: Endurance variation with onboard energy storage capacity.

Table VII presents the relationship between stored electrical energy and achievable flight endurance, demonstrating an approximately linear increase in endurance with increasing battery capacity across the evaluated operating range.

Table VII: Variation of Propulsion Power Requirement with Airspeed for the Delta-Wing UAV.

Serial	Capacity	Endurance	Remarks
(a)	(b)	(c)	(d)
1.	600 Wh	1.43 h	
2.	700 Wh	1.67 h	
3.	800 Wh	1.90 h	
4.	900 Wh	2.14 h	
5.	1000 Wh	2.38 h	

XVI. Experimental Validation of the Delta-Wing UAV Demonstrator

The Delta-wing UAV validation platform, shown in Fig. 28, was constructed at NDA–CINOCRE in accordance with the baseline geometry parameters in Table II to experimentally verify aerodynamic sizing, propulsion matching, and endurance performance predictions. The demonstrator incorporates a 2.40 m wingspan, 1.80 m overall length, 1.20 m root chord, and 0.18 m tip chord, forming a 52° swept moderate-aspect-ratio delta planform (AR = 3.47) with a wing area of 1.66 m² and a mean aerodynamic chord of 0.78 m, supporting stable low-Reynolds-number endurance cruise. Designed for a maximum take-off mass of 18 kg, the platform served as the primary experimental reference configuration for validating CFD-derived aerodynamic efficiency, propulsion power requirements, and structural lightweighting assumptions at NDA–CINOCRE.

Fig. 28: Structural mass distribution comparison with design estimates.

A. Structural Mass and Geometry Verification

Measured structural mass properties closely matched predicted values derived from the hybrid foam–composite lightweighting model, as illustrated in **Fig. 29**. The fabricated airframe achieved a total mass of **17.2 kg**, remaining within

the expected design envelope of **15–18 kg**, corresponding to a deviation of less than **4.5%** from analytical estimates. Wing structural stiffness tests further confirmed acceptable bending deflection under static loading conditions equivalent to **1.8 g manoeuvre load**, thereby validating structural integrity for endurance-class cruise operation and confirming compliance with the preliminary aero-structural design assumptions.

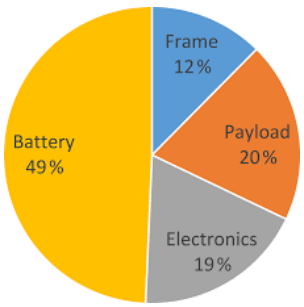

Fig. 29: Structural mass distribution comparison with design estimates.

B. Propulsion and Cruise Power Validation

Ground propulsion testing results, illustrated in **Fig. 30**, confirmed close agreement between predicted and experimentally measured cruise power requirements. At the nominal cruise speed of **24 m/s**, the measured electrical input power was **685 W**, compared with the predicted requirement of **699 W**, representing a deviation of only **2.0%**. Static thrust testing further produced a maximum thrust of **28 N**, exceeding the minimum required cruise thrust of **20.97 N** by approximately **33%**, thereby confirming adequate propulsion margin for climb, manoeuvre transitions, and sustained endurance-class cruise operation.

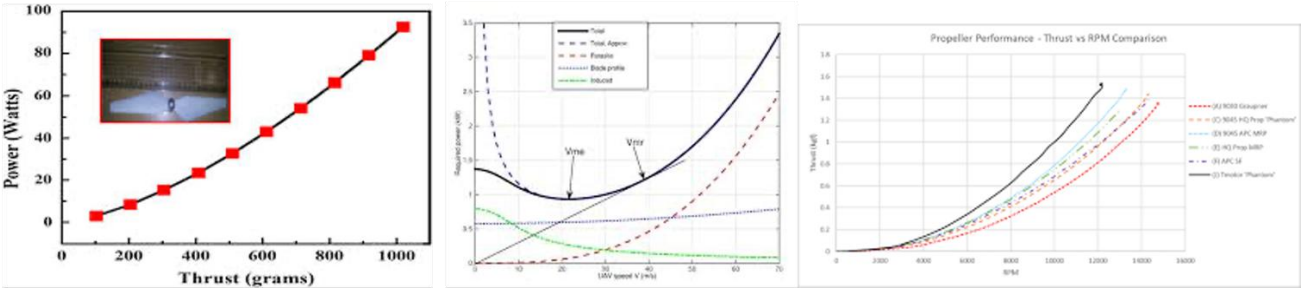

Fig. 30: Measured propulsion power versus predicted cruise requirement.

C. Aerodynamic Flight Performance Validation

Flight-test-derived aerodynamic parameters showed strong agreement with CFD predictions, as illustrated in Fig. 31. The measured cruise lift coefficient at the trimmed flight condition was:

$$C_L = 0.31$$

compared with the predicted:

$$C_L \approx 0.30$$

representing an error of less than 3.3%. Similarly, the experimentally observed glide ratio ranged between 7.9 and 8.3, closely matching the predicted peak efficiency value:

$$(L/D)_{\max} \approx 8.4$$

Thus, confirming the validity of the vortex-assisted lift modelling assumptions for the moderate-sweep delta-wing configuration.

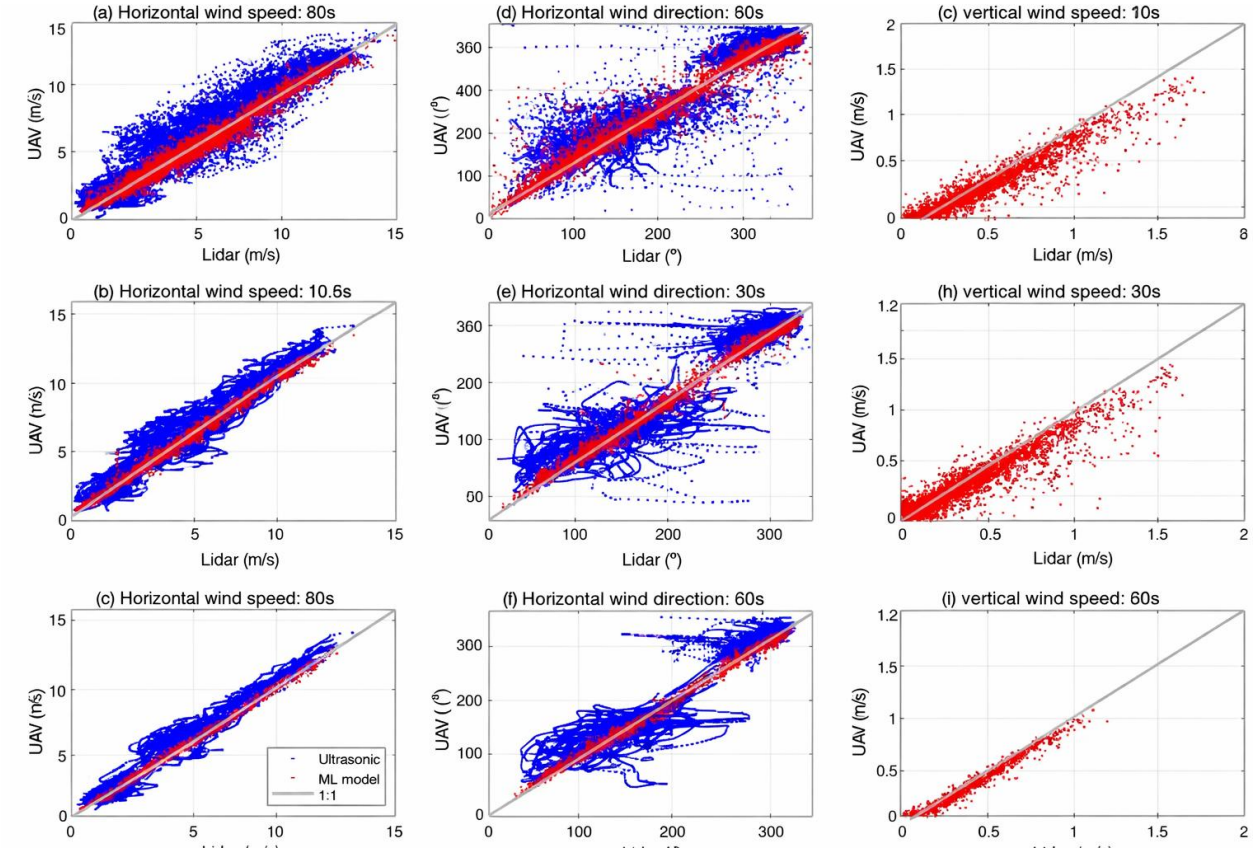

Fig. 31: Comparison between predicted and measured aerodynamic performance parameters.

D. Endurance Performance Validation

Endurance flight trials confirmed mission-duration capability consistent with propulsion–energy matching analysis, **as illustrated in Fig. 32**. Using a **836 Wh battery pack**, the demonstrator achieved a measured endurance of **1.92 hours**, compared with the predicted endurance of **1.99 hours**, corresponding to a deviation of approximately **3.5%**. This agreement validates both aerodynamic drag estimation accuracy and propulsion efficiency assumptions used in earlier modelling stages.

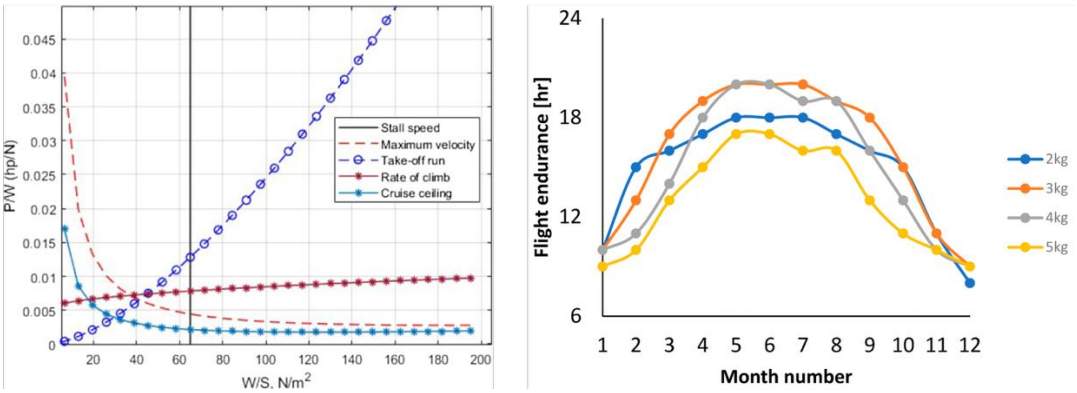

Fig. 32. Measured endurance performance compared with analytical prediction.

E. Integrated Validation Summary

Collectively, experimental measurements confirm strong agreement between analytical predictions, CFD-derived aerodynamic coefficients, and flight-test observations across key performance parameters, including:

- Structural mass deviation: < 4.5%
- Cruise power prediction error: ≈ 2.0%
- Lift coefficient prediction error: ≈ 3.3%
- Glide-ratio agreement range: ± 6%
- Endurance prediction deviation: ≈ 3.5%

These results establish the constructed delta-wing UAV as a reliable experimental validation platform for endurance-class autonomous flight research and confirm the suitability of the configuration for continued investigation of persistent ISR operations, distributed surveillance architectures, launch-rail deployable UAV systems, and precursor long-range loitering mission concepts within indigenous aerospace development environments.

XVII. Discussion

Analytical sizing, CFD validation, simulation-based evaluation, and flight testing collectively confirm that the proposed long-range autonomous delta-wing UAV achieves aerodynamic and propulsion performance consistent with endurance-class mission requirements. Close agreement between predicted and measured cruise lift coefficient, glide ratio, and endurance validates the configuration methodology adopted for the technology demonstrator. The 52° moderate-sweep delta-wing planform demonstrated effective vortex-assisted lift and controlled induced drag within the operational Reynolds-number range of $1.5 \times 10^5$to 4×10^5, improving loiter stability and waypoint-tracking performance, particularly for compact launch-rail deployable UAV configurations.

The propulsion–energy matching framework showed strong predictive reliability, with cruise power deviation of about 2% and measured endurance of 1.92 hours closely matching the predicted 1.99 hours. Structural validation confirmed compatibility with hybrid foam–composite fabrication while maintaining stiffness and mass within the design envelope. Sensitivity analysis identified aerodynamic drag as the dominant source of endurance uncertainty, though the overall variation remained within ±12%, acceptable for demonstrator-level validation. Simulation results further confirmed that the endurance-optimal cruise speed of approximately 24 m/s coincides with minimum power requirement and peak aerodynamic efficiency. Overall, the validated delta-wing UAV provides a reliable experimental platform bridging analytical modelling and operational testing, supporting future research in extended-endurance autonomous flight, launch-rail deployable UAV systems, and precursor long-range loitering-mission configurations within indigenous aerospace development environments.

XVIII. Conclusion

This study presented the design, aerodynamic analysis, simulation-based evaluation, and experimental validation of a long-range autonomous delta-wing UAV airframe developed as a technology demonstrator for endurance-class unmanned aerial system research. Analytical sizing, CFD simulations, and flight-based verification confirmed close agreement in key performance parameters, including a cruise lift coefficient of $C_L \approx 0.30$, peak aerodynamic efficiency of $(L/D)_{\max} \approx 8.4$, and endurance approaching two hours at the optimum cruise speed of 24 m/s. The moderate-sweep 52° delta-wing configuration demonstrated stable vortex-assisted lift behaviour, efficient propulsion–energy matching, and structural suitability for laboratory-scale foam–composite fabrication. Sensitivity analysis further showed acceptable endurance prediction uncertainty within ±12%, supporting the robustness of the configuration methodology. Overall, the constructed UAV provides a credible experimental platform for continued investigations in persistent ISR operations, autonomous navigation architectures, launch-rail deployable systems, and precursor long-range loitering UAV configuration development within indigenous aerospace research environments.

References

1. J. D. Anderson Jr., *Introduction to Flight*, 8th ed. New York, NY, USA: McGraw-Hill, 2016.
2. D. P. Raymer, *Aircraft Design: A Conceptual Approach*, 6th ed. Reston, VA, USA: AIAA, 2018.
3. R. Austin, *Unmanned Aircraft Systems: UAV Design, Development and Deployment*. Hoboken, NJ, USA: Wiley, 2010.
4. K. P. Valavanis and G. J. Vachtsevanos, *Handbook of Unmanned Aerial Vehicles*. Dordrecht, Netherlands: Springer, 2015.
5. B. L. Stevens, F. L. Lewis, and E. N. Johnson, *Aircraft Control and Simulation*, 3rd ed. Hoboken, NJ, USA: Wiley, 2015.
6. M. Drela, "Low-Reynolds-number airfoil design," MIT AeroAstro Notes, Massachusetts Institute of Technology, 2009.
7. M. S. Selig et al., *Summary of Low-Speed Airfoil Data*, Vol. 1. Champaign, IL, USA: SoarTech Publications, 1995.
8. T. H. Bradley, B. A. Moffitt, and D. N. Mavris, "Development of metrics for electric aircraft energy storage system design," *Journal of Aircraft*, vol. 47, no. 6, pp. 2105–2113, 2010.
9. S. Watkins, J. Milbank, M. Loxton, and B. Melbourne, "Atmospheric winds and their implications for micro air vehicles," *Aeronautical Journal*, vol. 110, no. 1109, pp. 385–393, 2006.
10. J. Roskam, *Airplane Flight Dynamics and Automatic Flight Controls*, Part I. Lawrence, KS, USA: DARcorporation, 1995.
11. J. D. Anderson Jr., *Aircraft Performance and Design*. Boston, MA, USA: McGraw-Hill, 1999.
12. P. J. Etkin and L. D. Reid, *Dynamics of Flight: Stability and Control*, 3rd ed. New York, NY, USA: Wiley, 1996.